Structure and organization of phospholipid/polysaccharide nanoparticles

2008 J. Phys.: Condens. Matter 20 104211

(http://iopscience.iop.org/0953-8984/20/10/104211)

J. Phys.: Condens. Matter **20** (2008) 104211 (8pp) doi:10.1088/0953-8984/20/10/104211

Structure and organization of phospholipid/polysaccharide nanoparticles

Y Gerelli[1], M T Di Bari[1], A Deriu[1], L Cantù[2], P Colombo[3], C Como[3], S Motta[3], F Sonvico[3] and R May[4]

[1] Dipartimento di Fisica and CNISM, Università degli Studi di Parma and CRS SOFT, INFM-CNR, Italy
[2] Dipartimento di Chimica, Biochimica e Biotecnologie per la Medicina—LITA, Università di Milano, Italy
[3] Dipartimento Farmaceutico, Università degli Studi di Parma, Italy
[4] Institut Laue-Langevin, Grenoble, France

E-mail: Antonio.Deriu@fis.unipr.it

Received 16 July 2007, in final form 1 November 2007
Published 19 February 2008
Online at stacks.iop.org/JPhysCM/20/104211

Abstract

In recent years nanoparticles and microparticles composed of polymeric or lipid material have been proposed as drug carriers for improving the efficacy of encapsulated drugs. For the production of these systems different materials have been proposed, among them phospholipids and polysaccharides due to their biocompatibility, biodegradability, low cost and safety. We report here a morphological and structural investigation, performed using cryo-TEM, static light scattering and small angle neutron and x-ray scattering, on phospholipid/saccharide nanoparticles loaded with a lipophilic positively charged drug (tamoxifen citrate) used in breast cancer therapy. The lipid component was soybean lecithin; the saccharide one was chitosan that usually acts as an outer coating increasing vesicle stability.

The microscopy and scattering data indicate the presence of two distinct nanoparticle families: uni-lamellar vesicles with average radius 90 Å and multi-lamellar vesicles with average radius 440 Å. In both families the inner core is occupied by the solvent. The presence of tamoxifen gives rise to a multi-lamellar structure of the lipid outer shell. It also induces a positive surface charge into the vesicles, repelling the positively charged chitosan molecules which therefore do not take part in nanoparticle formation.

1. Introduction

Nanoscience has been recently indicated as one of the most promising fields for technological innovation. Among other applications, nanotechnologies are expected to provide breakthrough improvements in healthcare and medicine. In particular therapy, regenerative medicine, diagnosis and drug delivery [1, 2] are expected to benefit from new nanomaterials. The need of new formulations for biotech drugs, as well as the opportunity of revaluing old drugs through new administration routes and innovative therapeutic applications, have given great impulse to the development of pharmaceutical nanotechnologies and microtechnologies. Indeed, their application allows the modification of the biopharmaceutic properties of drugs without changing their molecular structure; it is therefore an interesting approach for the administration of drugs presenting some hindering characteristics, such as low water solubility, rapid metabolism or elimination, narrow therapeutic index, toxic side effects. Several colloidal drug delivery systems have been proposed, as liposomes, micelles, nanoemulsions and nanoparticles. Polymeric and lipidic nanosystems improve drug bioavailability, modify pharmacokinetics or protect the encapsulated drug from enzymatic degradation. Some liposomal drugs have been approved or are under evaluation for clinical application, in particular for cancer treatment [3, 4]. Polymeric nanoparticles built up from biocompatible and biodegradable materials, such as poly(lactic acid) or poly(lactic-co-glycolic acid) have been investigated [5]. Synthetic polymers however are often insoluble in water and require the use of organic solvents for the manufacture of colloidal drug carriers. For this reason, great interest has been devoted

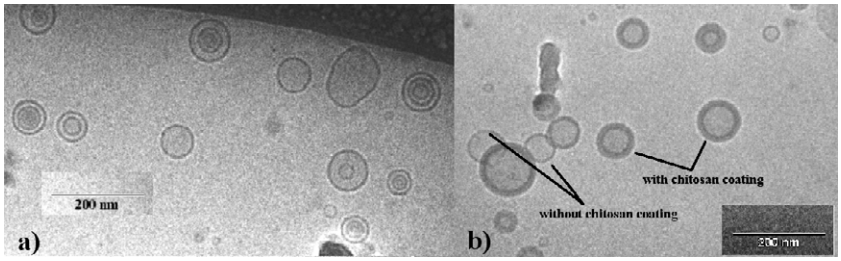

Figure 1. Cryo-TEM image of nanoparticles containing tamoxifen (panel (a)). The presence of two families (uni- and multi-lamellar vesicles) is evident, as well as a high overall polydispersity. In the multi-lamellar vesicles, the thickness $\langle t_c \rangle$ of the region between bilayers is also polydisperse. For comparison a cryo-TEM micrograph for nanoparticles loaded with a lipophilic non-charged drug (progesterone) is also shown (panel (b)). Their structure is similar to that of empty nanoparticles (data to be published).

to colloidal preparations obtained from biomaterials like polysaccharides and lipids that are considered biocompatible, biodegradable and safe. Recently, we have started a systematic investigation of the pharmaceutical [6] and physical–chemical [7] characteristics of new types of nanosystems obtained by self-assembling of phospholipids (soybean lecithin) and chitosan. Lecithin is a natural mix of phospholipids, obtained from soybean, composed mainly of phosphatidylcholine and phosphatidylethanolamine, that has been frequently used for liposome and micelle preparation [8, 9]. Chitosan, a cationic polysaccharide [poly-β-(1,4) glucosamine, $(C_6H_{11}O_4N)_n$] derived from chitin by deacetylation, is a versatile biomaterial with favourable biochemical properties: no toxicity, biocompatibility, biodegradability, bioadhesion [10, 11]. It has been proposed for a number of clinical and biomedical applications, ranging form scaffolds for tissue engineering to the production of colloidal drug carriers obtained by ionotropic gelation of the polymer with tripolyphosphate [12, 13]. Additionally, chitosan has been investigated for stabilization of microemulsions in which lecithin was one of the emulsifying agents [14]. In most of the cases reported in the literature, it turns out that the saccharide component acts as an outer coating that stabilizes the lipid vesicle structure. The lecithin/chitosan nanoparticles obtained with our preparation method are characterized by an hollow core surrounded by a lipid bilayer with a thin chitosan outer coating. This structure is observed in nanoparticles not containing drugs (void nanovectors), as well as in those loaded with a lipophilic non-charged drug (cryo-TEM image reported in figure 1; small angle neutron scattering data to be published). Here we present a structural investigation, performed by cryo-TEM (cTEM), static light scattering (SLS) and small angle scattering of neutrons (SANS) and x-rays (SAXS) on lecithin/chitosan nanoparticles in the presence of tamoxifen citrate, a lipophilic positively charged drug largely used in breast cancer therapy. Tamoxifen is a drug with a very low water solubility and a poor and erratic bioavailability after oral administration and therefore is expected to benefit from its formulation in biocompatible nanocarriers. Considering the lipophilic nature of this drug is it possible to hypothesize that its molecules will be mostly present into the lipid part of the investigated nanocapsules. This is a common feature of different kind of lipid–drug delivery systems [15–17]. A detailed knowledge of the changes in the nanoparticle structure due to the presence of the drug is important in order to optimize the loading efficiency and the kinetics of drug release.

2. Experimental details

2.1. Sample preparation and preliminary characterization

The main component of our system is Lipoid S45 (a commercial lecithin manufactured by Lipoid AG, Switzerland): a mixture of lipids, phospholipids and 30% of fatty acids with an overall negative charge. The second component is highly purified chitosan, a polysaccharide obtained by deacetylation of chitin which is positively charged at acid pH. The third component is tamoxifen citrate [18], a lipophilic drug used in breast cancer therapy, positively charged at acid pH. We started the preparation from two solutions: a first one composed by 200 mg of lecithin plus 60 mg of TAM all dissolved in 8 ml of methanol, a second one made up by 10 mg of chitosan diluted in 92 ml of water (H_2O or D_2O according to custom). Self-assembled nanoparticles were obtained by rapid injection (nozzle diameter 0.75 mm, injection rate 40 ml min^{-1}), under mechanical stirring, of the methanol solution into the aqueous one. The self-assembling process gave rise to a suspension of drug-loaded nanoparticles with concentration $c = 0.2\%$ w/w and pH $= 2.7$ [6]. It is worth noticing that TAM is already admixed with lecithin in the methanol solution while chitosan interacts whit lecithin only upon injection. For cTEM, SAXS and SLS measurements, the solvent was a mixture of pure H_2O (92%) and methanol (8%). For the SANS experiments two buffers were used: a perdeuterated one (D_2O 92% and D-methanol 8%), and a D_2O/H_2O mixture corresponding to the index matching of lecithin (73.7% H_2O, 18.3% D_2O, 8% H-methanol). In order to determine the mean hydrodynamic radius and the Z-potential (connected to the charge per unit surface area) a preliminary characterization was carried out by dynamic light scattering. Samples containing lecithin and lecithin/chitosan nanoparticles were also measured for comparison. The results are summarized in table 1. The particle morphology was investigated by cTEM experiments. cTEM is based on electron transmission microscopy on thin (≈5000 Å) vitrified aqueous films [19] obtained by cooling to liquid nitrogen temperature. The limiting factor, when using electrons as probes, is the small difference between the electronic density of amphiphilic molecules and that of the surrounding water; the experimental resolution can not therefore be higher than ∼40–50 Å. This corresponds to a typical bilayer thickness, therefore the internal bilayer structure can not be observed. Figure 1 shows cTEM micrographs for a typical suspension of TAM-loaded nanoparticles (panel (a)), and nanoparticles loaded with

Table 1. Comparison between average hydrodynamic radius ($\langle R_H \rangle$) and surface potential of lecithin vesicles (LEC), chitosan/lecithin nanoparticles (NCL) and those with TAM.

System	$\langle R_H \rangle$ (Å)	Polydispersity index (%)	Z-potential (mV)
LEC	350 ± 20	20	-48 ± 2
NCL	1140 ± 20	20	45 ± 2
NCL+TAM	670 ± 20	20	45 ± 3

progesterone, a non-charged lipophilic drug (panel (b)). The difference in structure is very evident: nanoparticles with progesterone are characterized by an hollow core surrounded by a lipid bilayer with a thin chitosan outer coating; this structure is very close to that observed in empty nanoparticles obtained with the same preparation method. In nanoparticles with TAM a multi-layered structure is clearly visible.

2.2. Static light scattering

The measurements were performed with a 677 nm incident wavelength covering a range of momentum Q from 3.0×10^{-4} to 2.4×10^{-3} Å^{-1}. Sample suspensions for SLS were diluted to a concentration $c = 0.04\%$ (w/w), adding water and 0.0001% of HCl in order to keep a constant pH. This was essential to avoid multiple scattering contributions.

2.3. Small angle neutron scattering

SANS experiments were performed at the Institut Laue-Langevin, ILL (Grenoble) using the D11 diffractometer. Three different wavelength, λ, and sample-to-detector distance, D, configurations were adopted ($\lambda = 5$ Å, $D = 5.5$ m; $\lambda = 5$ Å, $D = 20.5$ m; $\lambda = 10$ Å, $D = 34$ m) in order to cover a Q-range of about two decades from 9.4×10^{-4} to 0.1 Å^{-1}. Sample holders were standard quartz flat cells (1 mm thick). Standard corrections, cell subtraction and normalization to absolute scattering units were performed using ILL SANS routines.

2.4. Small angle x-ray scattering

SAXS data were collected at the ID02 beamline at the European Synchrotron radiation Facility, ESRF (Grenoble). Scattered x-rays ($\lambda = 1$ Å) were collected using a charge-coupled device (CCD). The sample-to-detector distance, D was 1.2 m; this configuration allows to explore a Q-range from 8×10^{-3} to 4×10^{-1} Å^{-1}. Calibration was performed using a silver behenate standard. Collected images were processed and corrected with the ID02 software; accurate background subtraction was performed by us at a later stage.

3. Data analysis

3.1. SLS and SANS

A simple low Q Guinier analysis was not feasible for both SANS and SLS data due to the high overall nanoparticle polydispersity (see figure 1). We therefore decided to assume

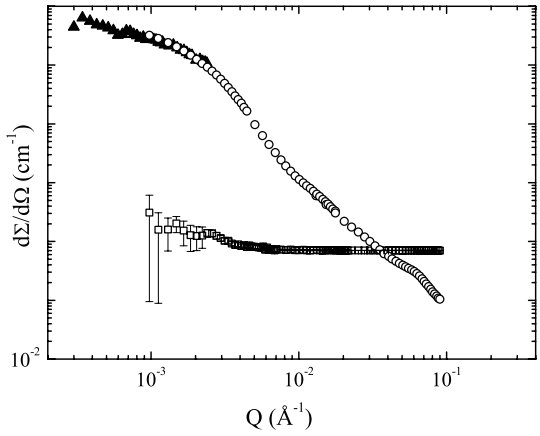

Figure 2. SANS and SLS profiles for the investigated nanoparticle solutions. SANS measurements in deuterated solvent (○) are in excellent agreement with the SLS ones (▲). SANS data at the lecithin matching point are also reported (□).

an analytical model for the scattering cross-section $d\Sigma(Q)/d\Omega$ suitable for the whole Q-range explored. Nanoparticle suspensions for the SLS experiments required a dilution higher than that used in SANS measurements (≈50 times). In order to properly match SLS and SANS data, we performed a preliminary SANS measure at the SLS concentration (0.04%, data not shown); these low concentration SANS data set can be perfectly superimposed to the higher concentration ones by re-scaling them according to their dilution ratio. This indicates that the overall size and structure of the nanoparticles are not appreciably influenced by dilution. The SANS curves were expressed in absolute scattering units and the SLS data were then normalized to the SANS ones obtaining a continuous curve covering almost three decades in Q (figure 2). The extremely good agreement of the SANS and SLS data in the overlap region has to be remarked. For a dilute solution of homogeneous and identical particles the scattered intensity $I(Q)$ is proportional to

$$\frac{d\Sigma(Q)}{d\Omega} = \frac{n}{V}\Delta\rho_p^2 |F(Q)|^2 \quad (1)$$

where n/V is the particle number density, $\Delta\rho_p \equiv \rho_p - \rho_s$ is the contrast between the scattering length density, SLD, of the particles (ρ_p) and of the solvent (ρ_s) [20]. In order to take into account the nanoparticle polydispersity the form factor $F(Q)$ has been weighted according to a Schultz distribution [21, 22], $D(\sigma, \langle R \rangle)$, with polydispersity index σ and centroid $\langle R_0 \rangle$. The differential scattering cross-section becomes therefore

$$\frac{d\Sigma(Q)}{d\Omega} = \frac{\phi}{\langle V \rangle}\Delta\rho_p^2 \int_0^{+\infty} dR\, D(\sigma, \langle R_0 \rangle) |F(Q, R)|^2. \quad (2)$$

Here the n/V in equation (1) is replaced by $\phi/\langle V \rangle$, where $\langle V \rangle$ is the mean particle volume according to the adopted distribution (for a Schultz distribution $\langle R^3 \rangle = (\sigma^2 + 1)(2\sigma^2 + 1)\langle R \rangle^3$) and ϕ is the particle volume fraction. The ratio $\phi/\langle V \rangle$ is then equal to the average particle number density. Guided by the morphological cTEM analysis, we adopted a model that takes into account both uni-lamellar (ULV) vesicles,

and multi-lamellar ones (MLV). The resulting differential cross-section is then the sum of two contributions shown in equation (3) and explained in detail in the following sections. A Q-independent background is also added to account for the incoherent scattering contribution from the hydrogens present in the sample

$$\frac{\mathrm{d}\Sigma(Q)}{\mathrm{d}\Omega} = p \times \frac{\phi}{\langle V_\mathrm{u}\rangle}\int_0^\infty D_\mathrm{u}(\sigma_\mathrm{u}, \langle R_0^\mathrm{u}\rangle)F_\mathrm{u}^2(Q, R)\,\mathrm{d}R + (1-p)\frac{\phi}{\langle V_\mathrm{m}\rangle}\int_0^\infty\Bigg[\mathrm{d}N D_\mathrm{m}(\sigma_\mathrm{m}, \langle N\rangle) \int_0^\infty \mathrm{d}t\, D(\sigma_\mathrm{c}, \langle t_\mathrm{c}\rangle)F_\mathrm{m}^2(Q, R(N,t))\Bigg] + bkg. \tag{3}$$

The subscripts u and m indicate the type of particles involved in each scattering contribution (ULV and MLV, respectively) and p is the relative population of ULV particles.

3.1.1. ULV particles. The model takes into account a polydisperse core (mean radius $\langle R_0^\mathrm{u}\rangle$), described by a Schultz distribution ($D_\mathrm{u}(\sigma_\mathrm{u}, \langle R_0^\mathrm{u}\rangle)$), surrounded by a shell with thickness t_B^u [23]. The total particle radius, $\langle R_0^\mathrm{u}\rangle + t_\mathrm{B}^\mathrm{u}$, has therefore the same polydispersity index (σ_u) as the core. The resulting form factor is

$$F_\mathrm{u}(Q, R) = 3\Delta\rho_\mathrm{B}^\mathrm{u}\left[V(R+t_\mathrm{B}^\mathrm{u})\frac{j_1(Q(R+t_\mathrm{B}^\mathrm{u}))}{Q(R+t_\mathrm{B}^\mathrm{u})} - V(R)\frac{j_1(QR)}{QR}\right] + 3\Delta\rho_0 V(R)\frac{j_1(QR)}{QR} \tag{4}$$

where j_1 is the spherical Bessel function of the first kind. The parameters of the ULV model are therefore the particle number density $\frac{p\times\phi}{\langle V_\mathrm{u}\rangle}$, the polydispersity index σ_u, the inner radius $\langle R_0^\mathrm{u}\rangle$, the lipid bilayer thickness t_B^u and the two contrasts, $\Delta\rho_0$ and $\Delta\rho_\mathrm{B}^\mathrm{u}$ for core and bilayer respectively.

3.1.2. MLV particles. In agreement with the morphological cTEM results, we assumed the contrast profile schematized in figure 3. It originates from an hollow core with radius R_0^m and contrast $\Delta\rho_0^\mathrm{m}$, a first bilayer with thickness t_B^m and contrast $\Delta\rho_\mathrm{B}^\mathrm{m}$ followed by a repetition of $\langle N\rangle - 1$ units, each composed by a solvent layer (thickness $\langle t_\mathrm{c}\rangle$ and contrast $\Delta\rho_0^\mathrm{m}$) plus a lipid bilayer. The particle polydispersity is due to the variable number of bilayers (described by the distribution $D_\mathrm{m}(\sigma_\mathrm{m}, \langle N\rangle)$) and to the polydispersity of the inter-layer thickness, $\langle t_\mathrm{c}\rangle$, described by a further Schultz distribution $D(\sigma_\mathrm{c}, \langle t_\mathrm{c}\rangle)$. The two above distributions (over $\langle N\rangle$ and over $\langle t_\mathrm{c}\rangle$) play a totally different role. The first one affects the external radius value and gives rise to a smearing of the SANS curve mostly near the Guinier region. The latter is needed to account for the width of the broad peak centred at $Q \approx 7\times10^{-2}$ Å^{-1} (see figure 2) and does not affect the mean total radius $\langle R_\mathrm{tot}\rangle$. The form factor for the MLV particles can then be expressed as

$$F_\mathrm{m}(Q, N, t) = 4\pi\,\Delta\rho_0^\mathrm{m}\int_0^{R_0^\mathrm{m}}\mathrm{d}R\,R^2\frac{\sin(QR)}{QR} + 4\pi\,\Delta\rho_\mathrm{B}^\mathrm{m}\int_{R_0^\mathrm{m}}^{R_0^\mathrm{m}+t_\mathrm{B}^\mathrm{m}}\mathrm{d}R\,R^2\frac{\sin(QR)}{QR}$$

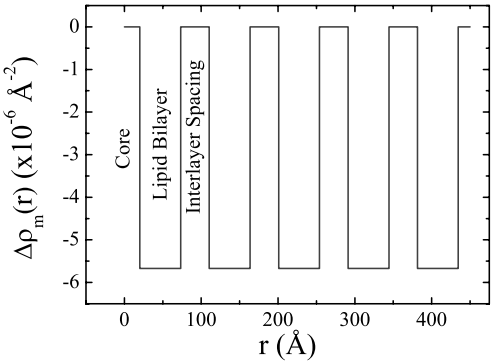

Figure 3. Radial SANS contrast profile adopted for multi-lamellar vesicle population (MLV).

$$+ 4\pi\sum_{j=0}^{N-1}\Bigg[\Delta\rho_0^\mathrm{m}\int_{R_j^0}^{R_j^c}\mathrm{d}R\,R^2\frac{\sin(QR)}{QR} + \Delta\rho_\mathrm{B}^\mathrm{m}\int_{R_j^c}^{R_{j+1}^0}\mathrm{d}R\,R^2\frac{\sin(QR)}{QR}\Bigg] \tag{5}$$

where the integration limits are

$R_j^0 = R_0^\mathrm{m} + (j+1)t_\mathrm{B}^\mathrm{m} + j\,t$
$\Rightarrow$ outer radius of the $(j+1)$th bilayer
$R_j^c = R_0^\mathrm{m} + (j+1)(t_\mathrm{B}^\mathrm{m} + t)$
$\Rightarrow$ outer radius of the $(j+1)$th solvent layer.

Equation (5) can be explicitly expressed in terms of spherical Bessel functions of the first kind, j_1, recalling that

$$4\pi\int_A^B \mathrm{d}x\,x^2\frac{\sin(Qx)}{Qx} = 3\left[\frac{4}{3}\pi B^3\frac{j_1(QB)}{QB} - \frac{4}{3}\pi A^3\frac{j_1(QA)}{QA}\right]. \tag{6}$$

For this model the parameters are: two polydispersity indices, σ_m and σ_c, the number of bilayers, $\langle N\rangle$, the core radius R_0^m, the thickness of the lipid layer and of the inter-layer (t_B^m and $\langle t_\mathrm{c}\rangle$ respectively) and the contrasts $\Delta\rho_0^\mathrm{m}$ and $\Delta\rho_\mathrm{B}^\mathrm{m}$. During the fit runs they were not all kept free at the same time. As explained in the following section, the results of the cTEM analysis and of first test of the model enabled us to fix some of them and to select well defined limits for other ones.

3.2. SAXS

SAXS experiments have been performed to exploit the different x-ray contrasts between lipid, saccharide and drug components of the nanoparticles and to extend the SANS upper Q-limit (0.1) to 0.4 Å^{-1}. In this way one can also investigate the internal structure of the lipid bilayers. In order to do this, we write the bilayer form factor as

$$F(Q, d) = \int_{-d/2}^{+d/2}\mathrm{d}x\,\Delta\rho(x)\cos(Qx) \tag{7}$$

where $d = 2(t_\mathrm{h} + t_\mathrm{t})$ is the bilayer thickness and $\rho(x)$ is the local electronic density across the bilayer. The x-dependent contrast $\Delta\rho(x)$ is described by a simplified head–tail model (see figure 4) [24], implying two uniform scattering

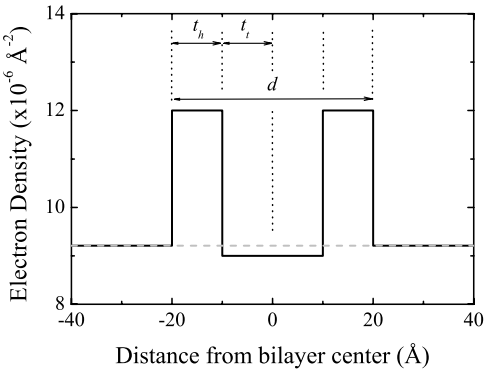

Figure 4. Electron density profile for the adopted head–tail model (——) and of the solvent (· · · · · ·). The head and tail thicknesses, t_h and t_t, and the total bilayer thickness, d, are also indicated.

length densities for the tail and for the head respectively. A more detailed description of $\Delta\rho(x)$ is not justified since the composition of the adopted commercial lipid (Lipoid S45) is partially unknown (see section 2.1). The SAXS intensity can therefore be expressed as

$$I(Q) = \frac{A}{Q^2} F^2(Q, d, \Delta\rho(x)). \tag{8}$$

Fitting parameters are: the scaling factor A and the thickness t_h and t_t (see figure 4). The routine used for the SAXS, SANS and SLS data is based upon an least square minimization from the MINUIT package [25].

4. Results and discussion

4.1. Nanoparticle structure

The cTEM micrographs (panel (a)) in figure 1 show the presence of two clearly different nanoparticle populations. Smaller nanoparticles (ULV, typical size about 20 nm) have a vesicular structure with a large hollow core and a relatively thin outer shell attributable to a single bilayer structure. From the micrographs one can infer a relatively large size polydispersity. Larger nanoparticles (MLV, typical size above 80 nm) have a clear multi-layer structure. They are as well polydisperse both in size and in number of layers. For MLV particles we have adopted the multi-layer model described previously and depicted in figure 3. Electronic contrast between water and saccharides is ten times bigger than that between water and lipids; cTEM can therefore provide information on the arrangement of chitosan. The cTEM micrographs suggest that chitosan is almost absent from the nanoparticles. This can be understood in terms of the nanocapsule preparation method: due to hydrophobic attraction, the lipophilic cationic TAM and the amphiphilic anionic lecithin, already admixed into the methanol solution, form mixed aggregates upon injection into the water/chitosan solution. The resulting positive charge of the resulting nanoparticles (see Z-potential values in table 1) inhibits surface adhesion of the positively charged chitosan molecules. Because of the acidity of the final solution (pH = 2.7), chitosan molecules in solution do not aggregate and keep elongated chain shapes [26].

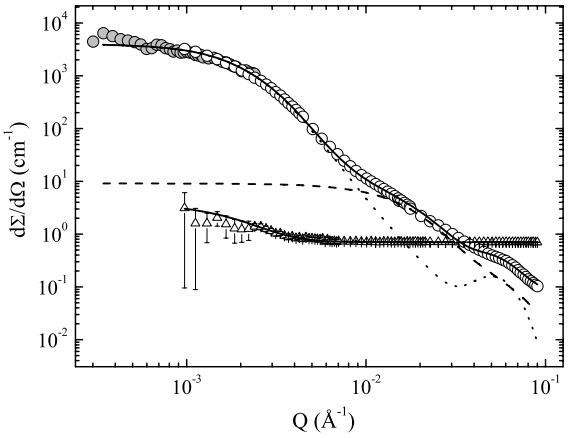

Figure 5. SANS data: (○) nanoparticles in deuterated solvent, (△) nanoparticles in lipoid-matched solvent, SLS (●) data. The continuous lines are the fits on both data sets to equation (9). The contributions of ULV (- - - -) and MLV (· · · · · ·) populations are also shown for nanoparticles in deuterated solvent.

Figure 5 shows the two SANS curves in absolute units for nanoparticle suspensions with concentration $c = 0.2\%$ (w/w) in both perdeuterated and lipoid-matched solvents. In the same figure the SLS data for a similar sample with $c = 0.04\%$ are reported after re-scaling to the SANS data. In the overlap region the agreement between the two curves is remarkable. It has also to be noted that a very small amount of much larger particles is likely to be present in the solution, as suggested by the discrepancy at very low Q between experimental SLS data and the fit. Their presence cannot be appreciated by SANS, restricted to higher Q, and they have therefore been neglected in the adopted model.

The two curves shown in figure 5 (SANS+SLS data for the sample in deuterated solvent and SANS data for the one in a solvent at the lipoid matching point) have been simultaneously fitted adopting the two-family model described in section 3.1.1 (see equation (3)). Preliminary fits, performed varying all the free parameters of the model, lead to the conclusion that the scattering contrasts $\Delta\rho_0$ and $\Delta\rho_0^{\mathrm{m}}$ are always very close to zero ($<10^{-14}$ Å^{-2}). This indicates that the core regions of both families and the inter-layer region of MLV nanoparticles are occupied by the solvent; these two contrasts were then set to zero in the subsequent analysis. Under this zero-contrast hypothesis the simultaneous fit of the data in figure 5 implies a system of two equations which differ only for the SLDs of the two solvents:

$$\begin{aligned}\frac{\mathrm{d}\Sigma(Q)}{\mathrm{d}\Omega} &= \frac{16\pi^2\phi}{Q^2}[p(\rho_{\mathrm{B}}^{\mathrm{u}} - \rho_{\mathrm{s}})^2 f_{\mathrm{u}}(Q) \\ &\quad + (1-p)(\rho_{\mathrm{B}}^{\mathrm{m}} - \rho_{\mathrm{s}})^2 f_{\mathrm{m}}(Q)] + bkg \\ \frac{\mathrm{d}\Sigma'(Q)}{\mathrm{d}\Omega} &= \frac{16\pi^2\phi}{Q^2}[p(\rho_{\mathrm{B}}^{\mathrm{u}} - \rho_{s'})^2 f_{\mathrm{u}}(Q) \\ &\quad + (1-p)(\rho_{\mathrm{B}}^{\mathrm{m}} - \rho_{s'})^2 f_{\mathrm{m}}(Q)] + bkg'\end{aligned} \tag{9}$$

where, apart from the contrast factors, $f_{\mathrm{u}}(Q)$ and $f_{\mathrm{m}}(Q)$ represent the form factors of the ULV and MLV families,

respectively,

$$f_u(Q) = \frac{1}{\langle V_u \rangle} \int_0^\infty dR\, D_u(\sigma_u, \langle R_0^u \rangle) \left| \int_0^R dr\, r\, \sin(Qr) \right|^2$$

$$f_m(Q) = \frac{1}{\langle V_m \rangle} \int_0^\infty \left\{ dN D_m(\sigma_m, \langle N \rangle) \int_0^\infty \left[dt\, D(\sigma_c, \langle t_c \rangle) \right. \right.$$

$$\left. \left. \left| \sum_{j=0}^{N-1} \int_{R_0^m + j(t+t_B^m)}^{R_0^m + j(t+t_B^m) + t_B^m} dr\, r\, \sin(Qr) \right|^2 \right] \right\}.$$

It has to be noted that equation (9) contains the product of the scattering contrast and the particle number density for both ULVs and MLVs. Nevertheless, since we work in absolute units and the SLD of both solvents are known, we can unambiguously determine the values of p and of the contrasts $\Delta\rho_B^m$ and $\Delta\rho_B^u$. From the cTEM micrographs the thickness parameters, t_b, t_b^m and $\langle t_c \rangle$ could be estimated; we could therefore put narrow limits to their range of variation, namely from 35 to 60 Å. cTEM provided also an initial guess for the relative population number, p and for the two polydispersity indices σ_m and σ_u. The curves resulting from the overall fit are shown as continuous lines in figure 5 together with the contributions of the ULV and MLV families. The results are summarized in table 2: they confirm that both ULV and MLV families are highly polydisperse. The values obtained for the lipid bilayer thicknesses t_B^u and t_B^m (≈50 Å) are in agreement with those typical for extruded pure lipid vesicles [24, 27, 28]. The SLD values indicate that in ULV particles the lipid bilayer is mostly composed by Lipoid ($\rho_{lipoid} \equiv \rho_{s'} = (0.59 \pm 0.06) \times 10^{-6}$ Å^{-2} as measured by index matching, $\rho_{tam} = 1.5 \times 10^{-6}$ Å^{-2} calculated),the amount of drug is zero within the experimental accuracy (≈0.08) in this case. On the other hand, from the SLD values obtained for MLV bilayers, it is possible to conclude that the drug/lipid ratio (w/w) is 0.20 ± 0.09. Overall, MLV nanoparticles are characterized by an average bilayer number $\langle N \rangle = 5$ with individual thickness t_b^m separated by inter-layer regions, with thickness $\langle t_c \rangle$, that are occupied by the solvent. This repetition leads to the broad peak observed in figure 5 at $Q \simeq 7 \times 10^{-2}$ Å^{-1}, its broadening being mainly due to the width of the $D(\sigma_c, \langle t_c \rangle)$ distribution. Indeed the average thickness of the multi-layer repeating unit $t_{tot} = \langle t_c \rangle + t_b^m = 90 \pm 24$ Å corresponds to $Q = 2\pi/t_{tot} = (7 \pm 2) \times 10^{-2}$ Å^{-1}. The average bilayer number $\langle N \rangle$, together with R_0^m, t_b^m, and $\langle t_c \rangle$ determine the mean external nanoparticle radius $\langle R_{tot} \rangle$ according to

$$\langle R_{tot} \rangle = R_0^m + t_B^m + [\langle N \rangle - 1]\left(\langle t_c \rangle + t_B^m\right) = 440 \text{ Å}.$$

The radius polydispersity index $\sigma_{tot} = 48\%$ is determined by the distribution in the number of bilayers $\langle N \rangle$.

4.2. Drug encapsulation

On the basis of the obtained SLD values, we can confirm that TAM is located within the lipid bilayers; this is not surprising if we consider the lipophilic nature of this drug. As explained before, TAM is mostly present into the MLV nanoparticles, with a 0.2–1 TAM to lecithin ratio (w/w). This ratio can be compared to the TAM/LEC one in the starting preparation (see section 2.1): 0.34–1. Taking into account the volume fraction of MLV nanoparticles, the effective loading efficiency (encapsulated drug/drug present in the starting solution) is (60 ± 10)%. This is in agreement with the loading capacity derived from the measured concentration of non-encapsulated drug extracted from the final solution by ultracentrifugation which is ≈60% [29]. This result is also confirmed by the contrast values resulting from the fit of the data described in section 4.1. After the flat incoherent background subtraction, the data at the lipoid matching point, are significantly different from zero only below $Q \simeq 0.025$ Å^{-1}. There the scattering signal is dominated by the MLV contribution; in fact $\Delta\rho_B^m(\text{matched}) \simeq 0.16$ and $\Delta\rho_B^u(\text{matched}) \simeq 0.040$ (see table 2); the scattered intensity is proportional to $(\Delta\rho)^2$ therefore the scattering signal arising from ULVs is negligible. The ratio between the scattering signals from the sample in deuterated solvent and from the one at the lipoid matching point is then: $[\Delta\rho_B^m(\text{deuterated})/\Delta\rho_B^m(\text{matched})]^2 = 1500$. This result is shown in figure 6 which shows a good superposition between data in deuterated solvent and the ones in the lipoid-matched solvent, once they are re-scaled by the above ratio. We have to remark that this comparison can be performed only below $Q = 0.025$ Å^{-1} i.e. in the region where the signal from the lecithin-matched samples, after subtraction of the flat incoherent background, is still appreciably ≠ 0.

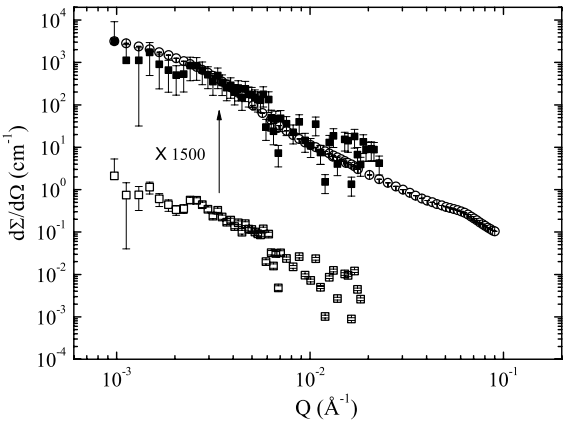

Figure 6. SANS curves for nanoparticles in deuterated (○) and lecithin-matched solvents (□). In both data sets a flat incoherent background has been subtracted. The latter data are also shown after re-scaling by a factor $[\Delta\rho_B^m(\text{deuterated})/\Delta\rho_B^m(\text{matched})]^2 = 1500$ (■).

Table 2. Fitting parameters obtained by equation (3) applied to SANS and SLS data.

		ULV	MLV
Core radius	$\langle R_0 \rangle$ (Å)	40 ± 2	20 ± 7
Polydispersity	σ (%)	∼50	—
Inter-layer thickness	$\langle t_c \rangle$ (Å)	—	37 ± 1
Polydispersity	σ (%)	—	∼23
Bilayer thickness	t_B (Å)	50 ± 5	53 ± 2
Bilayer SLD	ρ_B ($\times 10^{-6}$ Å^{-2})	0.59 ± 0.05	0.78 ± 0.08
Population in %		38	62

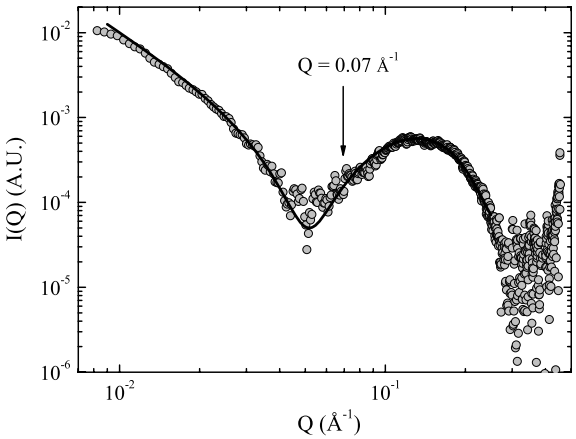

Figure 7. SAXS (●) data together with the fit according to equation (8) (——). The position expected for the low intensity peak due to the multi-lamellar periodicity is indicated.

Table 3. Fitting parameters obtained by equation (7) applied to ID02 data.

Zone	*SLD* ($\times 10^{-6}$ Å^{-2})	Thickness (Å)
Head	11 ± 1	11 ± 2[a]
Tail	9 ± 1	13.0 ± 0.5[a]

[a] Total bilayer thickness
$d = 2 \times (t_h + t_t) = 48 \pm 5$ Å.

4.3. Bilayer thickness

The SAXS analysis, performed in the range 8×10^{-3}–4×10^{-1} Å^{-1}, enabled us to investigate in more detail the structure of the lipid bilayer (see figure 7). In comparing the SANS and SAXS data one has to note that the low intensity peak at $Q \sim 0.07$ Å^{-1} observed in the SANS profile and due to the multi-lamellar periodicity is almost not visible in the SAXS curve. This fact is just accidental: the peak occurs close to the first minimum of the bilayer form factor in the x-ray data ($Q \sim 0.05$ Å^{-1}), while in the neutron case this minimum is expected at higher Q-values outside the range we investigated.

Owing to the partially unspecified composition of Lipoid S45, we have adopted a simplified description of the bilayer form factor leading to equation (7). The parameter values obtained from the fit are shown in table 3. The total bilayer thickness, $d \simeq 48$ Å agrees well with the one obtained from the SANS measurements and with literature values for the main lipid components of our lecithin [24, 27, 28].

5. Conclusion

The adopted nanoparticle preparation methodology (self-assembling following rapid injection of a lecithin+TAM methanol solution into a diluted aqueous solution of chitosan) gives rise to a polydisperse population characterized by two distinct families: uni-lamellar vesicles (ULV) with average radius 90 Å and multi-lamellar vesicles (MLV) with average radius 440 Å. In both families the inner core is occupied by the solvent. Tamoxifen is almost absent in ULV particles, while it is present in the MLV ones which have a loading efficiency around 60%. TAM molecules are located within each bilayer as expected for lipophilic molecules.

The presence of tamoxifen changes structure of the lipid outer shell from the uni-lamellar one observed in ULV particles, to a multi-lamellar with an average number of bilayers $\langle N \rangle = 5$ and a polydispersity index $\sigma_m = 48\%$. The thickness of a single lipid bilayer is similar in ULVs and in MLVs with a value close to that of pure DMPC [30], the main lipid component of lecithin. It seems therefore not to be affect by the presence of a charged drug and of a not negligible amount of fatty acids.

In lipid-based nanoparticles, chitosan acts usually as an outer coating that increases the vesicle stability. The introduction of a charged drug like tamoxifen induces a positive surface charge in the vesicles that repels the positively charged chitosan molecules which therefore do not take part in nanoparticle formation. Even in the absence of chitosan, the loaded nanoparticles show a stability sufficient for pharmaceutical applications [29]; this is probably due to the multi-lamellar assembly induced by the charged drug.

The choice of a multi-component commercial lipid mixture like Lipoid S45 was determined by the need of studying systems close to the ones used in pharmacological applications. The presence of 30% of fatty acids in Lipoid S45 can in principle additionally complicate the interpretation; we remark however that the matched solvent used in this experiment refers precisely to Lipoid S45 therefore, as concerns the scattering length densities, the presence of fatty acids is to some extent taken into account. The present analysis shows that careful morphological and structural characterization by complementary techniques like cTEM, SLS, SANS and SAXS can provided enough information to describe the main structural features of the particles and the effect of drug–particle interactions even when commercial components are adopted. In the next future we plan to extend this work towards nanoparticles in which commercial lecithin is replaced by a better-controlled binary lipid mixture. This should enable us to investigate in greater detail the lipid–solvent–drug interactions, and to better tailor these self-assembled systems for specific applications.

Acknowledgments

Many thanks to Mr S Barbieri for valuable help in sample preparation and for helpful discussions. The authors are grateful to Dr Göran Karlsson (University of Uppsala) for the cryo-TEM measurements. We also thank Dr E DiCola for her valuable technical assistance on the ID02 beamline at ESRF. Financial support by the Ministry of University and Research (PRIN founding framework) is gratefully acknowledged. Y Gerelli also acknowledges NMI3 for supporting his participation in ECNS 2007.

References

[1] Sonvico F, Dubernet C, Colombo P and Couvreur P 2005 *Curr. Pharm. Des.* **11** 2091–105
[2] Hughes G A 2005 *Nanomedicine* **1** 22–30

[3] Torchilin V P 2005 *Nat. Rev. Drug Discovery* **4** 145–60
[4] Kim K Y 2007 *Nanomedicine* **3** 103–10
[5] Csaba N, Sanchez A and Alonso M J 2006 *J. Control. Release* **113** 164–72
[6] Sonvico F, Cagnani A, Rossi A, Motta S, DiBari M T, Cavatorta F, Alonso M J, Deriu A and Colombo P 2006 *Int. J. Pharm.* **324** 67–73
[7] Sonvico F, DiBari M T, Bove L, Deriu A, Cavatorta F and Albanese G 2006 *Physica* B **385** 725–7
[8] Batzri S and Korn E 1973 *Biochim. Biophys. Acta* **298** 1015–9
[9] Felt O, Buri P and Gurny R 1999 *Drug Dev. Ind. Pharm.* **24** 979–93
[10] Illum L 1998 *Pharm. Res.* **15** 1326
[11] Singla A W and Chawla M 2001 *J. Pharm. Pharmacol.* **53** 1047
[12] Agnihotri S, Mallikarjuna N and Aminabhavi T 2004 *J. Control. Release* **100** 5–28
[13] Janes K, Calvo P and Alonso M 2001 *Adv. Drug Delivery Rev.* **47** 83–97
[14] Calvo P, Remunan-Lopez C, Vila-Jato J and Alonso M 1997 *J. Appl. Polym. Sci.* **63** 125–32
[15] Reddy L H, Vivek K, Bakshi H and Murthy R S 2006 *Pharm. Dev. Technol.* **11** 167–77
[16] Bondì M L, Craparo E F, Giammona G, Cervello M, Azzolina A, Diana P, Martorana A and Cirrincione G 2007 *Drug Delivery* **14** 61–7
[17] Riske K E, Cho S H, Lee H B, Jeong S Y and Yuk S H 2003 *J. Microencapsulation* **20** 489–96
[18] PubChem 2004 http://pubchem.ncbi.nlm.nih.gov/summary/summary.cgi?sid=17389724&viewopt=Deposited
[19] Almgren M, Edwards K and Karlsson G 2000 *Colloids Surf.* A **174** 3–21
[20] Sears V F 1992 *Neutron News* **3** 26–37
[21] Lee J H, Agarwal V, Bose A, Payne G F and Raghavan S R 2006 *Phys. Rev. Lett.* **96** 048102–1
[22] Kiselev M A, Wartewig S, Janich M, Lesieur P, Kiselev A M, Ollivon M and Neubert R 2003 *Chem. Phys. Lipids* **123** 31–44
[23] Bartlett P and Ottewill R H 1992 *J. Chem. Phys.* **96** 3306–18
[24] Riske K A, Amaral L Q and Lamy-Freund M T 2001 *Biochim. Biophys. Acta* **1511** 297–308
[25] Cern program library: http://cernlib.web.cern.ch/cernlib/
[26] Guo H F, Lin H L and Yu T L 2002 *J. Macromol. Sci.* A **39** 837–52
[27] Kučerka N, Pencer J, Sachs J N, Nagle J F and Katsaras J 2007 *Langmuir* **23** 1292–9
[28] Ristori S, Oberdisse J, Grillo I, Donati A and Spalla O 2005 *Biophys. J.* **88** 535–47
[29] Como C, Sonvico F, Rossi A, Corradini E and Colombo P 2006 *AAPS J. S2* **8** W4163
[30] Zemlyanaya E V, Kiselev M A and Aswal V K 2004 *Preprint* 0411029v2 [physics.chemph]